Bioorganic & Medicinal Chemistry 19 (2011) 1189–1196

Contents lists available at ScienceDirect

Bioorganic & Medicinal Chemistry

journal homepage: www.elsevier.com/locate/bmc

Identification of curcumin derivatives as human glyoxalase I inhibitors: A combination of biological evaluation, molecular docking, 3D-QSAR and molecular dynamics simulation studies

Minggui Yuan [a,†], Minxian Luo [a,†], Yao Song [b], Qiu Xu [a], Xiaofeng Wang [b], Yi Cao [b], Xianzhang Bu [a,*], Yanliang Ren [b,*], Xiaopeng Hu [a]

[a] School of Pharmaceutical Science, Sun Yat-sen University, Guangzhou 510006, China
[b] Key Laboratory of Pesticide & Chemical Biology (CCNU) of Ministry of Education, College of Chemistry, Central China Normal University, Wuhan 430079, China

ARTICLE INFO

Article history:
Received 17 November 2010
Revised 15 December 2010
Accepted 16 December 2010
Available online 22 December 2010

Keywords:
Glyoxalase I
Curcumin derivatives
3D-QSAR
Molecular docking
Molecular dynamic simulations

ABSTRACT

Several recent developments suggest that the human glyoxalase I (GLO I) is a potential target for anti-tumor drug development. In present study, a series of curcumin derivatives with high inhibitory activity against human GLO I were discovered. Inhibition constant (K_i) values of compounds **8, 9, 10, 11** and **13** to GLO I are 4.600 μM, 2.600 μM, 3.200 μM, 3.600 μM and 3.600 μM, respectively. To elucidate the structural features of potent inhibitors, docking-based three-dimensional structure–activity relationship (3D-QSAR) analyses were performed. Satisfactory agreement between experiment and theory suggests that comparative molecular similarity index analysis (CoMSIA) modeling exhibit much better correlation and predictive power. The cross-validated q^2 value is 0.638 while no-validation r^2 value is 0.930. Integrated with docking-based 3D-QSAR CoMSIA modeling, molecular surface property (electrostatic and steric) mapping and molecular dynamics simulation, a set of receptor-ligand binding models and bio-affinity predictive models for rational design of more potent inhibitors of GLO I are established.

1. Introduction

Glyoxalase system, composed of glyoxalase I (GLO I) and glyoxalase II (GLO II), is the main detoxification pathway in cancer, inflammatory cell and in normal cell.[1] Methylglyoxal (MGO), a by-product in glycolysis, is a cytotoxic substance, as it can conjugate covalently with DNA or protein to disable them in cell. As glutathione (GSH) is redundant in cell, the new produced MGO reacts with GSH to form conjugate methylglyoxal-glutathione (MGO-GSH), the latter is isomerized into lacticglutathione by GLO I, then GLO II catalyzes the hydrolysis of lacticglutathione into lactic acid and GSH.[1–3] Glyoxalase system is abnormally highly expressed in cancer cell as well as in inflammatory cell to evacuate the MGO immediately.[4–6] Thus, GLO I have been treated as the potent anti-cancer and anti-inflammatory targets for a long time, and have received more and more attentions recently.

Great efforts have been made to design, synthesize and develop the inhibitors of GLO I. For example, *S*-(*N*-hydroxy-*N*-P-iodophenylcarbonyl)-glutathione (HIPC-GSH),[2] *S*-(*p*-bromobenzyl) glutathione[7] have high inhibitory activities on GLO I. However, most of these compounds are derivatives of GSH and might be the prey of other enzymes, of which the cofactor or substrate is GSH. On the other hand, these compounds have poor kinetics properties as GSH is charged under physiological condition.[7,8] Non-glutathione compounds, such as Nonsteroidal Anti-inflammatory Drugs (NSAIDs),[9] methyl-gerfelin,[10] flavonoids,[11,12] and curcumin[13] were also reported having inhibitory affects on GLO I.

Curcumin is a polyphenol derived from the plant Curcuma longa.[13] Extensive researches revealed that curcumin exhibits a series of physiological functions, such as anti-virus, anti-infection, anti-tumor and anti-inflammatory activities,[14,15] by inhibiting the biological activity of GLO I (K_i = 5.1 μM).[13]

So far, four crystals of GLO I/inhibitor complex (1QIN,[2] 1QIP,[2] 1FRO,[16] and 2ZA0[10]) were determined, which not only cause to increase better understandings into GLO I structure and its catalysis mechanism, but also help to develop novel inhibitors with high inhibitory activities on GLO I and better pharmaceutical properties. It is interesting to design and synthesis GLO I inhibitors based on the structure of curcumin and properties of the active site.

The main purpose of this study was elucidate the interaction mechanism between the inhibitors and the active site of GLO I, to establish the rational bio-affinity predictive modes of more potent inhibitors of GLO I. In present study, a series of curcumin derivatives compounds were tested in vitro GLO I inhibitory assay, several compounds exhibit high inhibitory activity on GLO I. To increase the

* Corresponding authors.
E-mail addresses: phsbxzh@mail.sysu.edu.cn (X. Bu), renyl@mail.ccnu.edu.cn (Y. Ren).
† These authors contributed equally to this study.

0968-0896/$ - see front matter © 2010 Elsevier Ltd. All rights reserved.
doi:10.1016/j.bmc.2010.12.039

diversity of compounds, seven NSAIDs compounds were also employed. 3D-QSAR CoMSIA modeling shows good prediction power for experimental K_i values. One of the most active compounds was chosen to perform molecular dynamics (MD) simulation to further validate the proposed binding mode. The information would provide deep insights into interaction mechanism between inhibitors and active site of GLO I, to further develop novel, high selective inhibitors based on present rational receptor–ligand binding modes.

2. Material and methods

2.1. Materials

Compounds **1–20** (Fig. 1) are synthesized as reported previously,[17] and compounds **21–31** (Figs. 1 and 2) are purchased from the Sigma–Aldrich company.

2.2. Expression and purification of human glyoxalase I

The human GLO I gene was cloned from aUAMS-32 (stromal/osteoblastic cell line) cDNAlibrary by Funeng Gene Co. LTD (Guangzhou China), and subcloned into the pET15b (Invitrogen). The His-tag fusion proteins were expressed in the *Escherichia coli* BL21 (DE3) strain and purified on a HisTrap HP (GE Healthcare) according on manufacture.

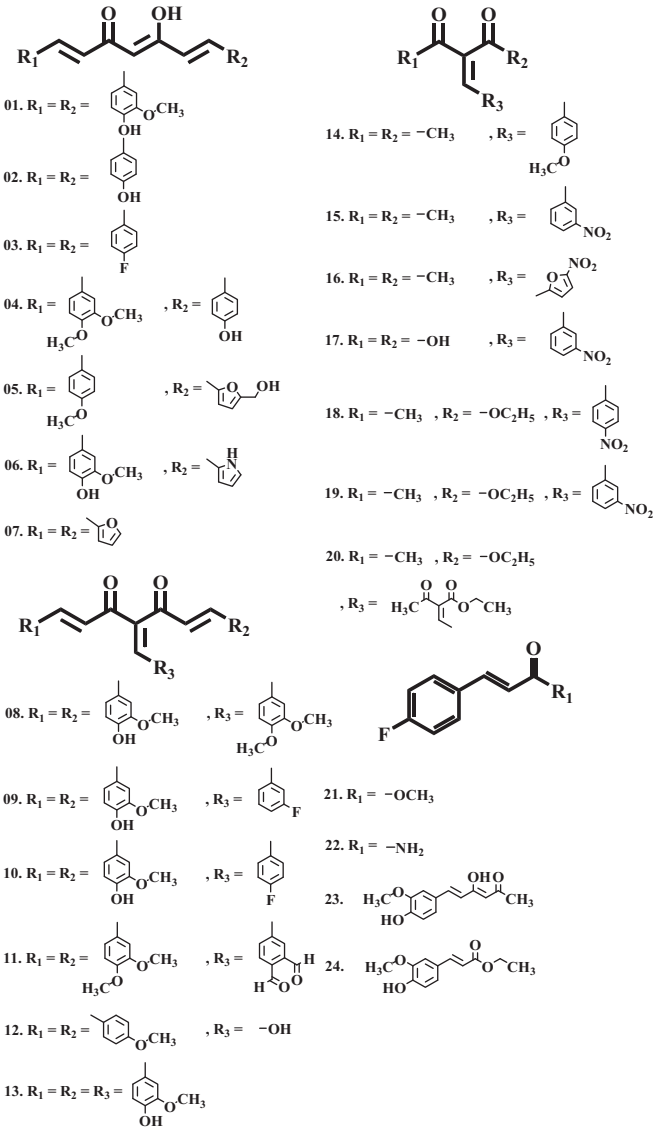

Figure 1. Molecular structural formulas of curcumin derivatives for the 3D-QSAR modeling.

2.3. Determination of the inhibition constants

The in vitro GLO I inhibitory assay was performed according to the previous report[3] but with some modifications. The reaction buffer contained 0.1 M sodium phosphate (pH 7.1) and hemithioacetal (MG-SG) was pre-incubated for 20 min at 30 °C. For the desired concentration of MG-SG, the concentrations of MG and GSH were calculated and varied by using the equation constant (K_d = 3 mM), and excess free GSH in the assay was kept 0.1 mM. The reaction was initiated by the addition of recombinant human His-GLO1 (35 mU) to the reaction buffer with or without compound. Spectrophotometer was used to monitor the initial velocity of the increase of absorbance at 240 nm as the formation of *S*-D-lactoylglutathione. The K_i values of the inhibitors were evaluated by Dixon plot showing the reciprocal of initial velocity versus the different inhibitor concentration at three substrate concentration (Fig. 3).

2.4. Molecular docking

The docking procedure is described as the previous article.[8,18] The structures of all compounds were prepared and docked into the crystal structure of GLO I (PDB ID: 1QIN) by using CDOCKER module of Accelrys Discovery Studio 2.1 suite (Accelrys Software Inc., San Diego, CA). HIPC-GSH was used to define the site sphere in binding site of GLO I, of which the radius was 8 Å from the centre. The docking parameters were retained default if not referred to. Finally, 10 poses were generated for each compound. The docking pose with the lowest CDOCKER interaction energy for each compound was selected as the optimal pose for further analyses.

2.5. Molecular dynamics (MD) simulations

To confirm binding mode of inhibitors, the MD simulations were performed using AMBER 10 package,[19] based upon the docked conformation of compound **8**. The partial atomic charges of ligands were calculated by using the restricted electrostatic potential (RESP)[20] fitting protocol implemented in the Antechamber module. A non-bonded approach was applied to Zinc ion whose interaction with protein was treated strictly through van der Wals and Coulomb forces.[21] AMBER ff99SB force field was used for protein parameters while general AMBER force field (GAFF) for the parameters of ligand. Na^+ ions were added to neutralize the system, and then solvated in an octahedral box of TIP3P water molecules,[22] which extended at least 10 Å from any given protein atom of GLO I. Prior to MD simulation, the complexes were subjected to 10,000 steps of energy minimization to relieve geometric strain and close intermolecular contacts. With weak constraint to the complex (10 kcal/mol), the system was gradually heated from 0 to 300 K in 50 ps and then equilibrated for 50 ps at 300 K using the NVT (constant composition, volume, and temperature) ensemble. Then, a 6 ns MD simulation was performed using periodic boundary conditions, with constant pressure and temperature (1 bar at 300 K). The temperature was kept at 300 K by means of the weak-coupling algorithm. The SHAKE algorithm was used to constrain bonds involving hydrogen atoms.[23] Particle Mash Ewald[24] was employed to calculate long-range electrostatic interaction. The non-bond cutoff was set at 10 Å. The output trajectories were recorded every 2 ps for the purpose of subsequent analysis. The equilibration was monitored by examining the stability of the temperature, energy, and the density of the system as well as the root-mean-squared deviations (RMSD) of the backbone atoms.

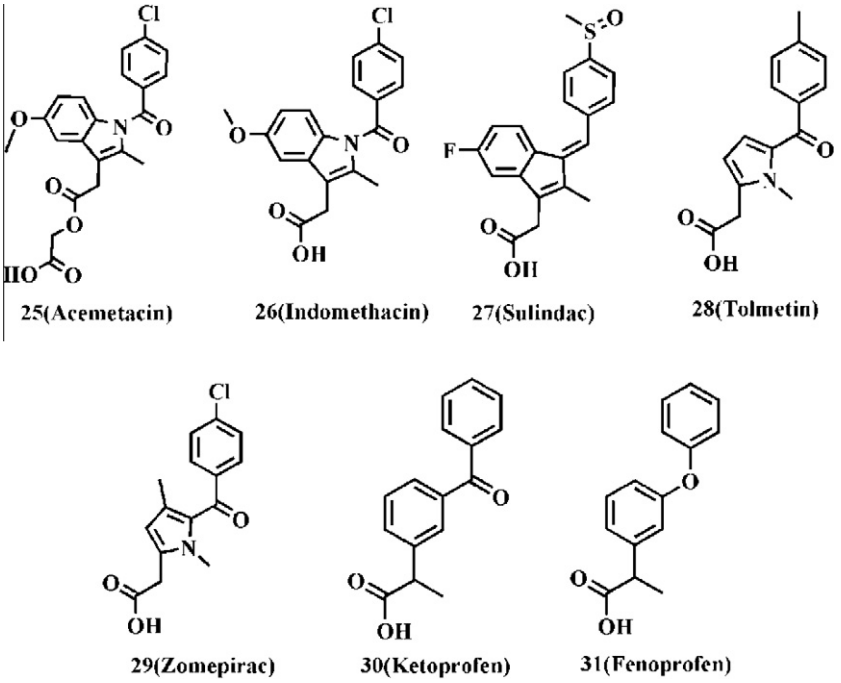

Figure 2. Molecular structural formulas of non-steroidal anti-inflammatory drugs used in present study.

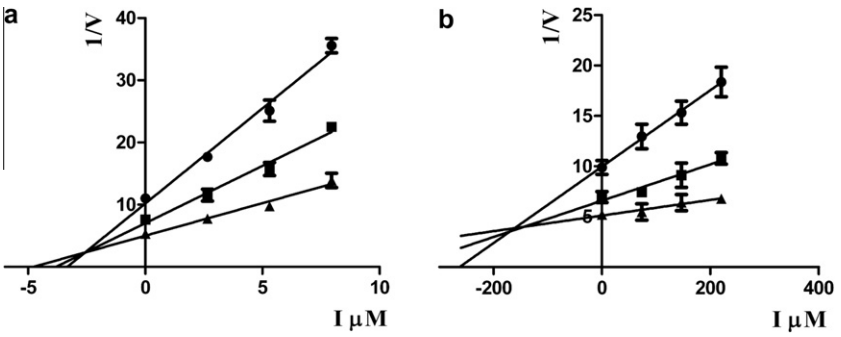

Figure 3. Dixon plots of glyoxalase I (GLO I) inhibition by compound **9** (a) and **18** (b), respectively. Purified GLO I (35 mU) was incubated with increasing concentrations of different inhibitors at 0.10 mM, 0.23 mM, 0.35 mM substrate concentrations; and enzyme activity was recorded (n = 3, SD <10%).

2.6. 3D-QSAR studies

To explore the specific contributions of steric, electrostatic, hydrophobic, hydrogen bond acceptor and donor[18] in binding modes for inhibitors with active site of GLO I, both CoMFA and CoMSIA studies were performed. The training sets were composed of 26 inhibitors with the pK_i value, and test sets comprised 5 compounds of data sets as list in Table 1. One of the important steps in developing 3D-QSAR modeling is the determination of active conformation and alignment of molecules. An efficient solution in this study is to depend on docking programs. The reliability of this methods have been documented in previous studies.[25,26] The alignment conformation of each molecule was the one with lowest interaction energy in the docked results of CDOCKER. Parameters of molecular docking simulation were as mentioned before.

2.6.1. CoMFA

Generally, steric and electronic field energies were probed using a sp^3 carbon atom and a +1.0 net charge atom,[27] respectively. And the steric and electrostatic interactions were calculated using the Tripos force field with a distance-dependent dielectric constant at all intersections in a regularly spaced (1 Å) grid. The column filter was set to 2.0 kcal/mol to improve the signal-to-noise ratio by omitting the lattice points which energy variation was below the threshold. The cutoff values of 20 kcal/mol was adopted for both steric and electrostatic field, and the regression analysis was carried out using the full cross-validated partial least squares (PLS) method (leave one out) with CoMFA standard options for scaling of variables. The final model (no-validation conventional analysis) was developed with the optimum number of components obtained in the cross-validated step.

2.6.2. CoMSIA

Similar to the CoMFA approach, a data table has been constructed from similarity indices calculated via the default probe. In the present study, five physicochemical properties, steric, electrostatic, hydrogen bond acceptor and hydrogen bond donor fields were evaluated using a Gaussian function. The attenuation factor was set to 0.3 as default.

2.6.3. Model validation

The predictive ability of CoMFA and CoMSIA modeling can be evaluated based on q^2, the cross-validated correlation coefficient, which qualifies the predictive ability of the models. Scrambled test

Table 1
Experimental, predicted inhibitory activity of 31 compounds by the CoMSIA methods based upon active conformation achieved by molecular docking

Compounds[a]	K_i[b] (μM)	pK_i/10[6]	Predicted pK_i/10[6c]	Residual error
1	10.00	4.987	5.262	0.2750
2	18.00	4.740	4.433	−0.3070
3	4.600	5.337	4.752	−0.5850
4	29.00	4.535	4.712	0.1770
5	74.00	4.133	4.470	0.3370
6	18.00	4.730	4.527	−0.2030
7	1500	3.824	4.122	0.2980
8	4.600	5.337	5.338	0.0010
9	2.600	5.585	5.502	−0.0830
10	3.200	5.495	5.516	0.0210
11	3.600	5.444	5.244	−0.2000
12	109.0	3.962	4.140	0.1780
13	3.600	5.444	4.954	−0.4900
14	383.0	3.417	3.230	−0.1870
15	91.00	4.041	4.279	0.2380
16	27.00	4.569	4.316	−0.2530
17	426.0	3.370	3.597	0.2270
18	159.0	3.800	4.310	0.5100
19	65.00	4.188	4.364	0.1760
20	39.00	4.412	4.066	−0.3460
21	1907	2.720	2.782	0.0620
22	1394	2.856	2.617	−0.2390
23	90.00	4.046	3.572	−0.4740
24	385.0	3.414	3.416	0.0020
25	49.00	4.312	4.274	−0.0380
26	24.00	4.613	4.543	−0.0700
27	139.0	3.858	3.918	0.0600
28	1014	2.994	3.003	0.0090
29	335.0	3.475	3.056	−0.4190
30	843.0	3.074	3.366	0.2920
31	383.0	3.417	3.268	−0.1490

[a] Underlined compounds were selected randomly to the test sets while the rest ones were in the training sets.
[b] Inhibition on GLO I was significantly different with respect to that of the control, $N = 3$, $P < 0.05$.
[c] Predicted activity values were derived from the CoMSIA modeling.

(Y scrambling) was performed to investigate the risk of chance correlations. The inhibitory potencies of 31 compounds were randomly reordered for 30 times and subject to leave-one-out validation test, respectively. The average q^2 value was calculated. It is expected that the scrambled models should have significantly lower q^2 values than the proposed one.[28] The models were also validated by test sets, in which the compounds are not included in the training sets. Usually, one can believe that the modeling is reliable, when the q^2 and r^2 for test sets is larger than 0.5 and 0.6, respectively. Criteria of k, the slope of the regression line between experimental and the prediction biological activities should range between 0.85 and 1.15.

3. Results and discussion

3.1. Activity assay

The structures and the corresponding K_i values of all tested compounds were shown in Figures 1 and 2 and Table 1, respectively. Kinetic analysis showed that all compounds exhibited a competitive-type inhibition pattern. Dixon-plot of compounds **9** and **18** are showed in Figure 3 as examples. The K_i values of curcumin, bisdemethoxycurcumin and NSAIDs were reported previously.[8]

Experimentally, a little structural modification on substituent of phenyl ring would strikingly affect the activity of two-ring curcumin derives (**1–7**), the K_i value is changed from 4.6 μM to 150 μM. The fluoride substituent on the phenyl ring increases inhibitory activity on GLO I, which lead to the compound **3** exhibit higher K_i (4.6 μM) than compound **1** (10.0 μM) and compound **2** (18.0 μM). When the methoxy group was taken into account, the K_i value of compound **1** is increased to 10 μM compared to those of compound **2** (18 μM). The K_i values of three-ring curcumin derives (**8–11**, **13**) are around 2.6–4.6 μM compared to compound **12**, which reveals that the third ring is structural favorable to the active site. Acetonic analogs (compounds **14–20**) were designed to imitate three-ring curcumin derives, they however failed to exhibit satisfactory inhibitory activity, which indicated that linkers and phenyl rings were both necessary for maintaining activity. For a comparison of compounds **3**, **21** and **24**, the remarkable changes of K_i value strongly indicated that 1,3-dicarbonyl group or its enol form as well as aromatic rings have critical contributions to the inhibitory activity. The inhibition constant of NSAIDs (**25–31**) were tested in the same condition with curcumin derivatives. For these compounds, the K_i values determined in present study were somewhat different from those reported previously,[9] except for the compound **28** (as compared in Table 2). For compound **28**, our experimental K_i (1014 μM) is about 10-fold higher than reported K_i (87.80 μM),[9] the predicted pK_i value using CoMSIA modeling however exhibit satisfactory consistent with our experimental values (Table 1). The positive results lend credit to the reliability of our experimental K_i values and CoMSIA modeling.

3.2. Binding model analyses

3.2.1. Molecular docking

CDOCKER docking results show that curcumin derivatives coordinated with Zn^{2+} in the active site of GLO I through oxygen atoms of carbonyl group; one terminal was buried into hydrophobic pocket site; the other was situated at the opening of active sites of GLO I, forming one or more hydrogen bonds with surrounding important residues (see Fig. 4).

It was demonstrated in our previous paper that the enol form of curcumin was the more stable conformation when binding with GLO I.[8] Asymmetric curcumin derivatives, such as compounds **4**–**6**, could exist two isomers (as shown in Fig. 5). The one with lower interaction energy in docking result was chosen, in which hydroxyl group of enol consistently closed to the opening site. A similar binding mode also can be exhibited by the two-ring curcumin derivatives, such as compounds **1**–**7**. Oxygen atoms of carbonyl group coordinated with Zn^{2+} in the active site. While one of the aromatic rings occupied the hydrophobic pocket, the other stretches to the H-bond binding region, the hydroxyl group can form H-bonds with residues Lys156, Arg122 or Arg37 (Fig. 4a). To some extent, inhibitory activity of the two-ring curcumin derivatives was affected by the substituent on aromatic rings, compounds which can form stronger H-bonds with residues in the hydrophobic pocket and H-bond binding region exhibit higher inhibitory activities, such as compounds **1** and **3**.

The shape of active site in GLO I is like the letter 'Y'. The three-ring curcumin derivatives, such as **8, 9, 10, 11** and **13** shared similar binding model (Fig. 4b). Two rings lay in the opening of the active site, the third buried into hydrophobic pocket site. The shape

Table 2
The comparison of experimental K_i values of the NSAIDs

No.	Compounds	K_i (μM)	K_i[a] (μM)
25	Acemetacin	49.00	12.90
26	Indomethacin	24.00	18.10
27	Sulindac	139.0	77.90
28	Tolmetin	1014	87.80
29	Zomepirac	335.0	107.0
30	Ketoprofen	843.0	414.0
31	Fenoprofen	383.0	400.0

[a] K_i values were derived from the paper published previously.[9]

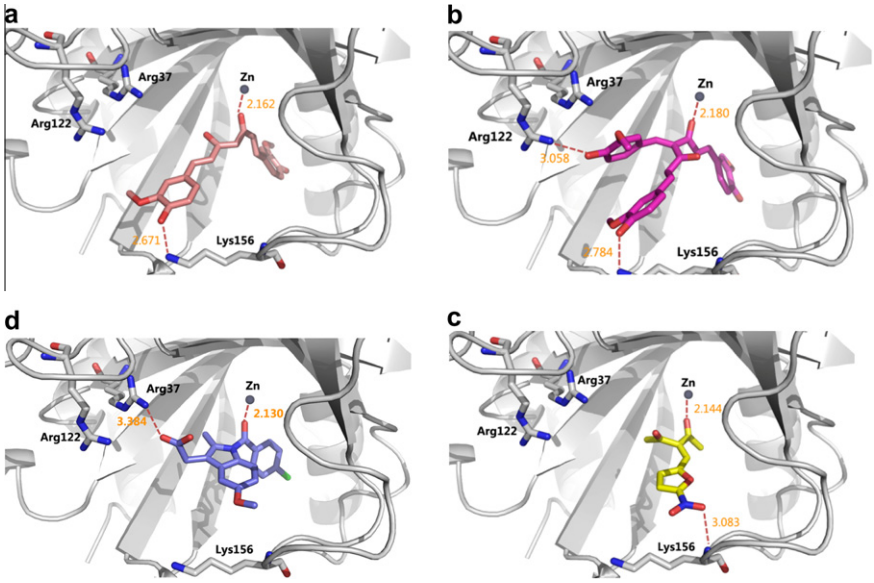

Figure 4. Optimal binding model of compounds **1, 8, 16** and **26** into active site of GLO I docked by CDOCKER, GLO I is shown in ribbon, ligands and some important residues are shown in stick, both coordination bonds and hydrogen bonds are shown in dashed lines (red). (a) Compound **1** (pink). (b) Compound **8** (magenta). (c) Compound **16** (yellow). (d) Compound **26** (blue).

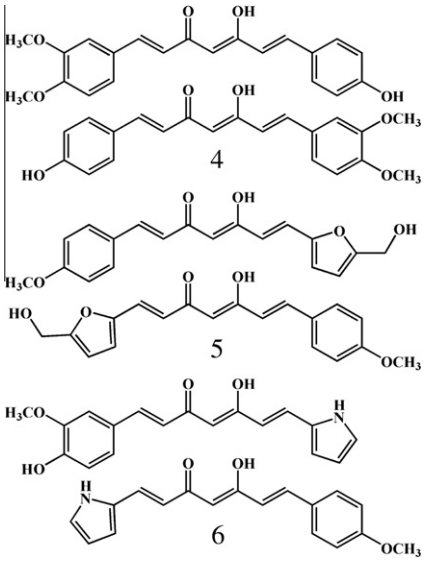

Figure 5. The isomers structure of compounds **4, 5** and **6**, which were docked into the active site of GLO I (PDB: 1QIN) by using CDOCKER module. For each compound, the one with the lowest interaction energy values was selected as the optimal conformation for further 3D-QSAR analyses.

similarity between the active site and these compounds could partially explain the high inhibitory of the three-ring curcumin derivatives.

Binding model of the acetonic derivatives (compounds **14–20**) were similar to the three-ring curcumin derivatives but the inside aromatic ring and one of the outside ring were missed. Oxygen atoms of inner carbonyl group coordinate with Zn^{2+} while the aromatic ring between two carbonyl groups lay in one side of entrance to form half of 'Y' shape (Fig. 4c).

Most of the non-steroidal anti-inflammatory drugs (compounds **25–29**) could coordinate with Zn^{2+} in active site through their carbonyl group oxygen atoms. The hydrophobic aromatic ring (if exists) was held tightly into hydrophobic pocket, while carbonic terminal located in the opening site (Fig. 4d).

3.2.2. Molecular dynamics (MD) simulations

In the docking studies, flexibility of the protein was not considered. To confirm binding models of ligands and to give a whole impression about the 3-ring curcumin derivatives, compound **8**, was subjected to 6 ns MD simulations. Average backbone RMSD of receptor was 1.094 Å with respect to the starting structure (Fig. 6a).

Average conformation was derived from 5.8 ns to 6.0 ns in simulation trajectory (Fig. 7). For complex 1QIN/compound **8**, there are two important hydrogen bonds: one is between hydroxyl oxygen atom of compound **8** and the nitrogen atom (named NH2) in residue Arg37, with a distance of 3.038 Å (Fig. 6b). Figure 6c shows the variation of distance between hydroxyl oxygen of the compound **8** inside the hydrophobic pocket and carbonyl oxygen of residue Met179, original hydrogen bond disappeared but a new and stable one was formed. The average distance from Zn^{2+} to outer carbonyl oxygen of compound **8** was about 2.095 Å during 6 ns simulation, which suggested that coordinate bond was stable (Fig. 6d). Pi–pi stacking interaction is observed between phenyl ring (R1) of the ligand and residue Phe67. Furthermore, some important residues in the active site of GLO I, such as Leu69, Phe71, Met157, Leu160, Leu182 and Met179, have hydrophobic interactions with the ligands, which could form a classic hydrophobic pocket. Compared with molecular docking results, MD results of compound **8** (Fig. 7) show a similar binding mode, lending credit to the reliability of active conformations obtained by CDOCKER module.

3.2.3. 3D-QSAR analyses

For CoMFA, interaction fields are represented as steric and electrostatic interaction energies calculated using Lennard–Jones potential and Coulombic potential for a molecule in the data set at the intersections of a grid embedding that molecule.[29] CoMSIA modeling uses Gaussian functions to describe the similarities of steric, electrostatic, hydrophobic, and hydrogen bond donor and acceptor properties.[30] With different shapes of the Gaussian function, the similarity indices can be calculated at all grid points, both inside and outside the molecular surface. The statistical details are summarized in Table 3. The underlined compounds in Table 1 were selected into test sets and the rest were in training sets. The cross-validated q^2 values of CoMFA and CoMSIA for training sets were

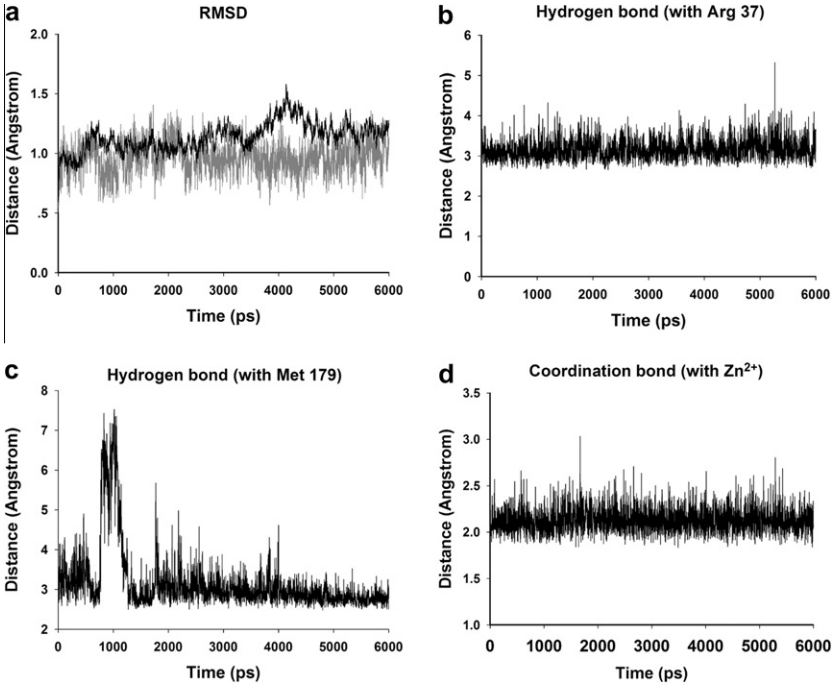

Figure 6. The results of MD simulation. (a) The MD simulation time vs root mean-square deviation (RMSD, in Å) of the backbone atoms (C, N, and C_α) for GLO I enzyme (black) and compound **8** (gray). (b) The intermolecular distance from O7 of compound **8** to Arg37. (c) The hydrogen bond from O6 of compound **8** to Met179. (d) The stable distance of coordination bond, from zinc to carboxyl oxygen of compound **8**, is around 2.000 Å.

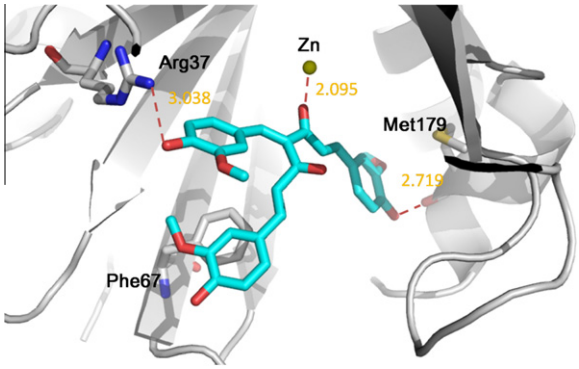

Figure 7. Average conformation of GLO I (1QIN) and compound **8**, which was derived from the last 100 conformations in 6 ns MD simulation. Coordination bond and hydrogen bonds are shown in dashed line (red). Compound **8** (cyan) forms stable coordination bond with zinc (yellow). After MD simulation, new hydrogen bonds with Arg37 and Met179 are formed, respectively, while original hydrogen bond with Arg122 is broken.

Table 3
Statistical characteristic of 3D-QSAR modeling

	CoMFA	CoMSIA
Training sets[a]		
q^2	0.608	0.634
r^2	0.954	0.930
pc	3	3
S	0.196	0.244
F	154.131	97.471
Contribution[b]	S:E = 0.611:0.389	S:H:A = 0.297:0.463:0.240
Test sets		
q^2	0.356	0.727
r^2	0.723	0.915
k	0.897	0.944

[a] Statistical parameters: q^2, cross-validated correlation coefficient; r^2, non-cross-validated correlation coefficient; *S*, standard error of estimate; *pc*, optimum number of components.
[b] Fields: S, steric; E, electrostatic; H, hydrophobic; D, hydrogen-bond donor; A, hydrogen-bond acceptor.

0.608 and 0.634, respectively. The non-cross-validated PLS analysis yielded r^2 values of 0.954 and 0.930, respectively. Optimum number of components (PC) of both models was 3. Predicted pK_i values of 31 compounds by CoMFA and CoMSIA modeling have been given in Table 1. The well agreement between predicted pK_i value and experimental pK_i value for both test sets and training sets using CoMSIA modeling are shown in Figure 8. The higher q^2 (0.727), R^2 (0.915) and k (0.944) for test sets can be achieved by CoMSIA modeling, we therefore believe that CoMSIA modeling shows more satisfactory prediction ability than CoMFA modeling. It is conclude that CoMSIA modeling was more reasonable to reveal the structural–activity relationship of inhibitors binding to GLO I. Average q^2 of scrambled test was −0.2669 for CoMSIA modeling. CoMSIA analysis suggests that the steric, hydrophobic, hydrogen-bond acceptor field distributions were 29.7%, 46.3%, 24.0%, respectively. It is indicated that hydrophobic interaction dominate the binding between these compounds and GLO I, which is in agreement with the binding model discussed in molecular docking.

In CoMSIA modeling, the steric fields are represented by green- and yellow-colored contours (green, bulky substituent favored; yellow, bulky substituent disfavored); the hydrophobic fields are represented by cyan- and white-colored contours (cyan, favored; while white disfavored); the hydrogen-bond acceptor fields are denoted by magenta and red contours (magenta, favored; while red, disfavored).

The S1 region in steric contour is located in hydrophobic pocket of active site of GLO I, where the bulkier substituent is preferred in these regions (Fig. 9a). As it was mentioned before, the shape of the active site of GLO I is like the letter 'Y'. However, the two arms are not so symmetric. Another bulkier favorable region S2 is located in the large arm of 'Y', which is in the opening area of the active site. There is an important NS region lies in the smaller arm of 'Y' (Fig. 9c). One phenyl ring of compound **8** can hit to the NS region,

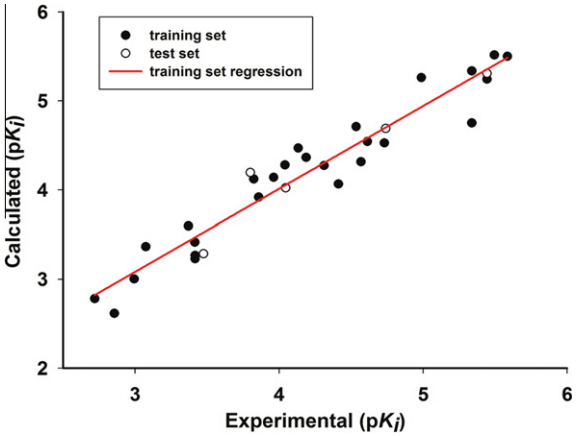

Figure 8. The predicted versus experimental pK_i value for the inhibition of GLO I. The predicted pK_i values were generated using CoMSIA modeling based on 'SHA' fields.

the other two rings full filled into S1, S2 regions. Smaller compounds, such as compound **21** and **22**, however lose to fill the bulkier favorable region (Fig. 9b). That is one of the explanations that the inhibition activities of compounds **8–11** is 103-fold higher than those of compounds **21** and **22**, and around 3–5-fold higher than two rings curcumin derivatives, such as compounds **1** and **2**. Aromatic rings of compounds **14**–**20** fill S2 region, but R2 substituent do not fit S1 region so well that they still exhibit moderate inhibitory activities. These analyses are in well consistence with the molecular docking results.

In CoMSIA hydrophobic contour plots, a large hydrophobically favored region, H1, located in the hydrophobic pocket surrounded by residues Leu69, Phe71, Met157, Leu160, Leu182 and Met179 in the active site of GLO I (Fig. 9d). Aromatic rings presented in this region lead to hydrophobic interaction increase, thus two-ring and three-ring curcumin derivatives (compounds **1–3**, **8–11** and **13**) and some non-steroidal drugs, such as indomethacin and acematacin, exhibit high inhibitory activity. Another hydrophobic favor region H2 present in the 'large arm' of 'Y-shape' active site, one of phenyl rings of 3-ring curcumin derivatives (compound **8**) located this region can form pi–pi stacking interaction with nearby Phe67 residue. It is in consistence with MD simulation results (Fig. 7). The two white regions (NH1 and NH2) where hydrophilic groups are favored, locate inner of hydrophobic pocket and the shorter arm of 'Y', respectively. In these regions, the hydrophilic substituent, such as hydroxyl, is preferred. Take compound **8** for example, methoxy group of inner phenyl ring presents in NH1 region, which is in contrary to contour map property. Thus, the methoxy group in NH1 region should be replaced by hydroxyl group to increase inhibitory activity on GLOI. In NH2 region, most of the compounds in the present study possess the hydrophilic group.

In CoMSIA hydrogen bond acceptor field contour plot, there is one hydrogen bond acceptor favored region (A1) in the large arm of 'Y-shape' active site, surrounded by Arg122 and Asn103 (Fig. 9e). Thus, hydroxyl group (R1 group) of compounds **1, 2, 8, 9, 10, 13,** etc can form hydrogen bond with these amino acids. In contrast, the compounds **7** and **12** exhibit lower inhibitor activity because there is no strong hydrogen-bond acceptor at its R1 group position. Another hydrogen bond acceptor favored region (A2) located in the middle of the active site, where the outer carbonyl group or hydroxyl group of the inhibitors is present. These groups are the common structure of the inhibitors in the present study, unfortunately, the remarkable interactions for this group with important residues is still could not found in docking results, their function are still uncertain. The NA region locates at the phenyl

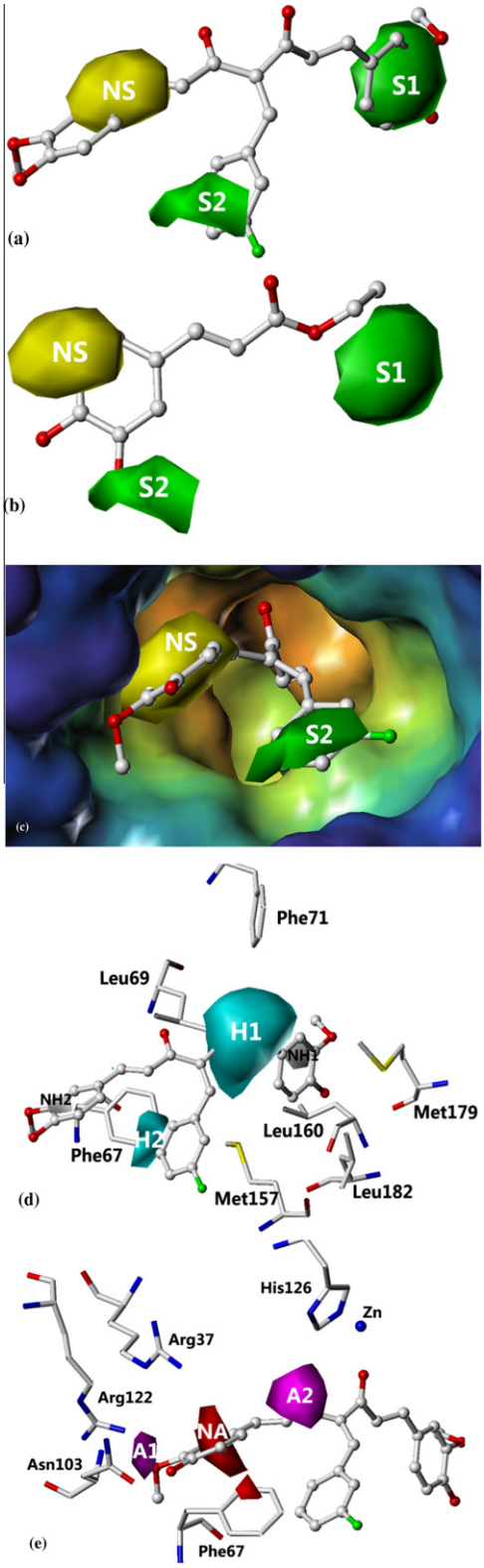

Figure 9. The contour maps from the CoMSIA modeling. Compound **9** (a, c, d, e) and compound **24** (b) are shown in ball and stick, the important residues are shown in stick. (a, b) Sterically favored areas (85% contribution) are represented by green polyhedra and disfavored areas (5% contribution) are represented by yellow polyhedra. (c) The asymmetric opening of the Y-shape active site is displayed in cavity depth modes combined with sterical contour maps. (d) Hydrophobically favored areas (88% contribution) are represented by cyan polyhedra and disfavored areas (5% contribution) are represented by white polyhedra. (e) Hydrogen bond acceptor functionally favored regions (95% contribution) are represented by magenta polyhedra and disfavored regions (3% contribution) are represented by red polyhedra.

ring of R1 substitute, where hydrogen bond acceptors are not favored. Thus, in this region, the favored group is not furan but Phenyl group. It is the reason why compound **7** exhibited weak inhibitory activity. R1 group of compounds **14–22** is too short to fit into A1 and NA region; this is the appropriate explanation of their moderate to weak inhibitory activity.

4. Conclusion

In summary, the inhibition constants of 26 curcumin derivatives, as well as 7 NSAIDs on GLO I were determined. Some curcumin derivatives (**8–11** and **13**) exhibit high inhibitory activity. Molecular docking simulation was used to produce possible binding poses for these compounds to GLO I. MD simulation was performed to confirm the reasonable binding model of GLO I/compound **8** complex. Based on the molecular docking results, the 3D-QSAR modeling was performed to give further validation of the binding mode and provide a structural framework for understanding the structure–activity relationship of these compounds. Satisfactory agreement between experiment and theory suggests that comparative molecular similarity analysis (CoMSIA) modeling exhibit much better correlation and predictive power. The positive results indicated that the modeling strategies in present study most like to be an encouraging way in elucidation of protein–ligand interaction and rational design of novel GLO I inhibitors.

Acknowledgments

The authors gratefully thank National Basic Research Program of China (973 Program; Nos. 2010CB126100), the Natural Science Foundations of China (No. 30800169, 20873049, 20872044), the PCSIRT (No. IRT0953), the Research Fund for the Doctoral Program of Higher Education of China, 200805581146 and the self-determined research funds of CCNU from the colleges' basic research and operation of MOE (No. CCNU09A01010).

References and notes

1. Padmanabhan, P. K.; Mukherjee, A.; Madhubala, R. *Biochem. J.* **2006**, *393*, 227.
2. Cameron, A. D.; Ridderstrom, M.; Olin, B.; Kavarana, M. J.; Creighton, D. J.; Mannervik, B. *Biochemistry* **1999**, *38*, 13480.
3. Thornalley, P. J.; Edwards, L. G.; Kang, Y.; Wyatt, C.; Davies, N.; Ladan, M. J.; Double, J. *Biochem. Pharmacol.* **1996**, *51*, 1365.
4. Jones, M. B.; Krutzsch, H.; Shu, H. J.; Zhao, Y. M.; Liotta, L. A.; Kohn, E. C.; Petricoin, E. F. *Proteomics* **2002**, *2*, 76.
5. Rulli, A.; Carli, L.; Romani, R.; Baroni, T.; Giovannini, E.; Rosi, G.; Talesa, V. *Breast Cancer Res. Treat.* **2001**, *66*, 67.
6. Samadi, A. A.; Fullerton, S. A.; Tortorelis, D. G.; Johnson, G. B.; Davidson, S. D.; Choudhury, M. S.; Mallouh, C.; Tazaki, H.; Konno, S. *Urology* **2001**, *57*, 183.
7. Creighton, D. J.; Zheng, Z. B.; Holewinski, R.; Hamilton, D. S.; Eiseman, J. L. *Biochem. Soc. Trans.* **2003**, *31*, 1378.
8. Liu, M.; Yuan, M.; Luo, M.; Bu, X.; Luo, H. B.; Hu, X. *Biophys. Chem.* **2010**, *147*, 28.
9. Sato, S.; Kwon, Y.; Kamisuki, S.; Srivastava, N.; Mao, Q. A.; Kawazoe, Y.; Uesugi, M. *J. Am. Chem. Soc.* **2007**, *129*, 873.
10. Kawatani, M.; Okumura, H.; Honda, K.; Kanoh, N.; Muroi, M.; Dohmae, N.; Takami, M.; Kitagawa, M.; Futamura, Y.; Imoto, M.; Osada, H. *Proc. Natl. Acad. Sci. U.S.A.* **2008**, *105*, 11691.
11. Klopman, G.; Dimayuga, M. L. *Mol. Pharmacol.* **1988**, *34*, 218.
12. Takasawa, R.; Takahashi, S.; Saeki, K.; Sunaga, S.; Yoshimori, A.; Tanuma, S. I. *Bioorg. Med. Chem.* **2008**, *16*, 3969.
13. Santel, T.; Pflug, G.; Hemdan, N. Y.; Schafer, A.; Hollenbach, M.; Buchold, M.; Hintersdorf, A.; Lindner, I.; Otto, A.; Bigl, M.; Oerlecke, I.; Hutschenreuter, A.; Sack, U.; Huse, K.; Groth, M.; Birkemeyer, C.; Schellenberger, W.; Gebhardt, R.; Platzer, M.; Weiss, T.; Vijayalakshmi, M. A.; Kruger, M.; Birkenmeier, G. *PLoS One* **2008**, *3*, e3508.
14. Goel, A.; Kunnumakkara, A. B.; Aggarwal, B. B. *Biochem. Pharmacol.* **2008**, *75*, 787.
15. Joe, B.; Vijaykumar, M.; Lokesh, B. R. *Crit. Rev. Food Sci.* **2004**, *44*, 97.
16. Cameron, A. D.; Olin, B.; Ridderstrom, M.; Mannervik, B.; Jones, T. A. *EMBO J.* **1997**, *16*, 3386.
17. Qiu, X.; Du, Y.; Lou, B.; Zuo, Y.; Shao, W.; Huo, Y.; Huang, J.; Yu, Y.; Zhou, B.; Du, J.; Fu, H.; Bu, X. *J. Med. Chem.* **2010**, *53*, 8260.
18. Parrill, A. L.; Echols, U.; Nguyen, T.; Pham, T. C.; Hoeglund, A.; Baker, D. L. *Bioorg. Med. Chem.* **2008**, *16*, 1784.
19. Case, D. A.; Darden, T. A.; Cheatham, T. E.; Simmerling, C. L.; Wang, J.; Duke, R. E.; Luo, R.; Crowley, M.; Walker, R. C.; Zhang, W.; Merz, K. M.; Wang, B.; Hayik, S.; Roitberg, A.; Seabra, G.; Kolossvary, I.; Wong, K. F.; Paesani, F.; Vanicek, J.; Wu, X.; Brozell, S. R.; Steinbrecher, T.; Gohlke, H.; Yang, L.; Tan, C.; Mongan, J.; Hornak, V.; Cui, G.; Mathews, D. H.; Seetin, M. G.; Sagui, C.; Babin, V.; Kollman, P. A. *Amber 10*; University of California, 2008.
20. Wang, J. M.; Wang, W.; Kollman, P. A. *Abstr. Am. Chem. Soc.* **2001**, *222*, U403.
21. Stote, R. H.; Karplus, M. *Proteins* **1995**, *23*, 12.
22. Jorgensen, W. L.; Chandrasekhar, J.; Madura, J. D.; Impey, R. W.; Klein, M. L. *J. Chem. Phys.* **1983**, *79*, 926.
23. Krautler, V.; Van Gunsteren, W. F.; Hunenberger, P. H. *J. Comput. Chem.* **2001**, *22*, 501.
24. Nam, K.; Gao, J. L.; York, D. M. *J. Chem. Theory Comput.* **2005**, *1*, 2.
25. Zhang, Q.; Yang, J.; Liang, K.; Feng, L.; Li, S.; Wan, J.; Xu, X.; Yang, G.; Liu, D.; Yang, S. *J. Chem. Inf. Model.* **2008**, *48*, 1802.
26. Zhang, Q. Y.; Wan, J.; Xu, X.; Yang, G. F.; Ren, Y. L.; Liu, J. J.; Wang, H.; Guo, Y. *J. Comb. Chem.* **2006**, *9*, 131.
27. Avila, C. M.; Romeiro, N. C.; da Silva, G. M.; Sant'Anna, C. M.; Barreiro, E. J.; Fraga, C. A. *Bioorg. Med. Chem.* **2006**, *14*, 6874.
28. Gramatica, P.; Pilutti, P.; Papa, E. *J. Chem. Inf. Comput. Sci.* **2004**, *44*, 1794.
29. Cramer, R. D.; Patterson, D. E.; Bunce, J. D. *J. Am. Chem. Soc.* **1988**, *110*, 5959.
30. Klebe, G.; Abraham, U.; Mietzner, T. *J. Med. Chem.* **1994**, *37*, 4130.